ACS OMEGA

http://pubs.acs.org/journal/acsodf

Article

Surface Epitaxial Nano-Topography Facilitates Biomineralization to Promote Osteogenic Differentiation and Osteogenesis

Guan-Yin Zhu,[§] Ya-Hui Liu,[§] Wei Liu, Xin-Qi Huang, Bo Zhang, Zi-Li Zheng, Xin Wei, Jia-Zhuang Xu,* and Zhi-He Zhao*

Cite This: *ACS Omega* 2021, 6, 21792−21800

Read Online

ACCESS | Metrics & More | Article Recommendations | Supporting Information

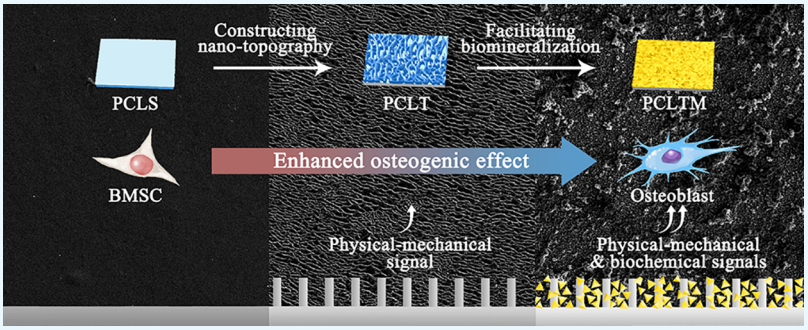

ABSTRACT: Biomimetic modification of hydroxyapatite on a polymer surface is a potent strategy for activating biological functions in bone tissue engineering applications. However, the polymer surface is bioinert, and it is difficult to introduce a uniform calcium phosphate (CaP) layer. To overcome this limitation, we constructed a specific nano-topographical structure onto a poly(ε-caprolactone) substrate via surface-directed epitaxial crystallization. Formation of the CaP layer on the nano-topological surface was enhanced by 2.34-fold compared to that on a smooth surface. This effect was attributed to the abundant crystallization sites for CaP deposition because of the increased surface area and roughness. Bone marrow mesenchymal stromal cells (BMSCs) were used to examine the biological effect of biomineralized surfaces. We clearly demonstrated that BMSCs responded to surface biomineralization. Osteogenic differentiation and proliferation of BMSCs were significantly promoted on the biomineralized nano-topological surface. The expression of alkaline phosphatase and osteogenic-related genes as well as extracellular matrix mineralization was significantly enhanced. The proposed strategy shows potential for designing bone repair scaffolds.

INTRODUCTION

Bone defects are a common clinical problem caused by trauma, developmental deformities, tumor resection, and infection, among other factors. When a bone defect area exceeds a critical size, the body cannot heal itself, necessitating clinical intervention.[1] Currently, autologous and allogeneic bone allografts are the commonly used treatment approaches. However, these two approaches have some limitations, such as donor site damage, infection, limited bone transplantation volume, and high cost.[2−5] Thus, additional methods for bone regeneration are needed.

Bone tissue engineering (BTE) is an advanced method used to overcome the primary limitations of traditional treatments. Using this approach, we seeded cells, such as mesenchymal stem cells (MSCs), onto scaffold implants where MSCs differentiate into osteoblasts to promote bone regeneration. This method has multiple advantages, such as low infection risk, excellent biocompatibility, and no apparent complications.[6−8] However, seeded cells (particularly stem cells) often exhibit multilineage differentiation ability, and guiding their osteogenic differentiation is key to bone regeneration.[9] Thus, obtaining detailed insights into bone physiology and constructing BTE scaffolds with good osteoconductivity and osteoinductivity are necessary.[10,11]

Considering the inorganic and organic composition of natural bone tissues, a wide variety of biomaterials and their combinations have been evaluated as candidates for BTE applications, such as polymers, bioceramics, and composite materials.[12] Among these, aliphatic polyester materials, such as poly(ε-caprolactone) (PCL), poly(lactic-*co*-glycolic acid), and poly(L-lactic acid), have attracted attention because of their excellent biocompatibility, plasticity, degradability, abundance and easy availability of sources, and low cost.[13−17] However, unlike the natural extracellular matrix (ECM), these polyesters

Received: July 1, 2021
Accepted: August 5, 2021
Published: August 13, 2021

https://doi.org/10.1021/acsomega.1c03462
ACS Omega 2021, 6, 21792−21800

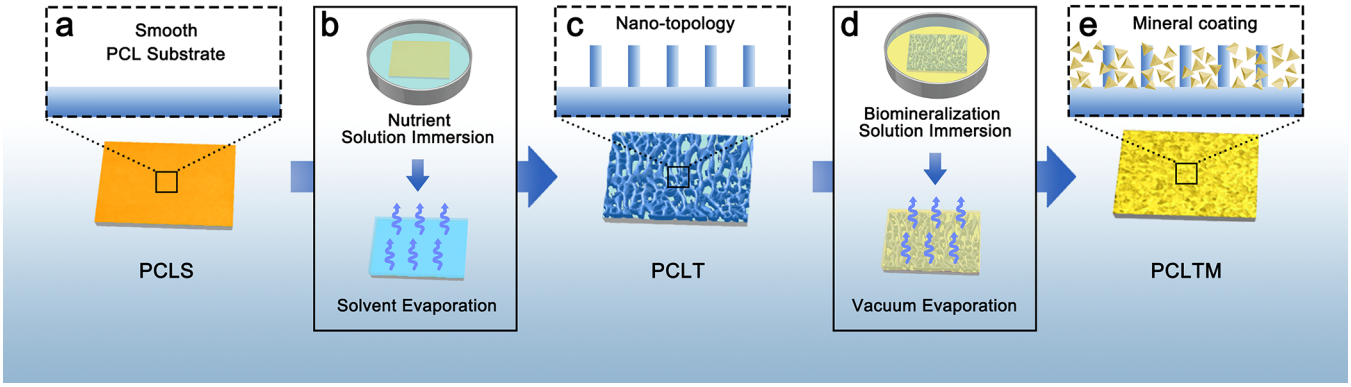

Figure 1. Schematic illustration of biomineralization on the nano-topology surface: (a) PCL substrate with a smooth surface (PCLS). (b) Immersion of PCLS into nutrient solution followed by solvent evaporation. (c) Formation of the nano-topology surface on the substrate (PCLT). (d) Immersion of PCLT into biomineralization solution (SBF) followed by vacuum evaporation. (e) Formation of the biomimetic mineralized layer onto the nano-topology surface (PCLTM).

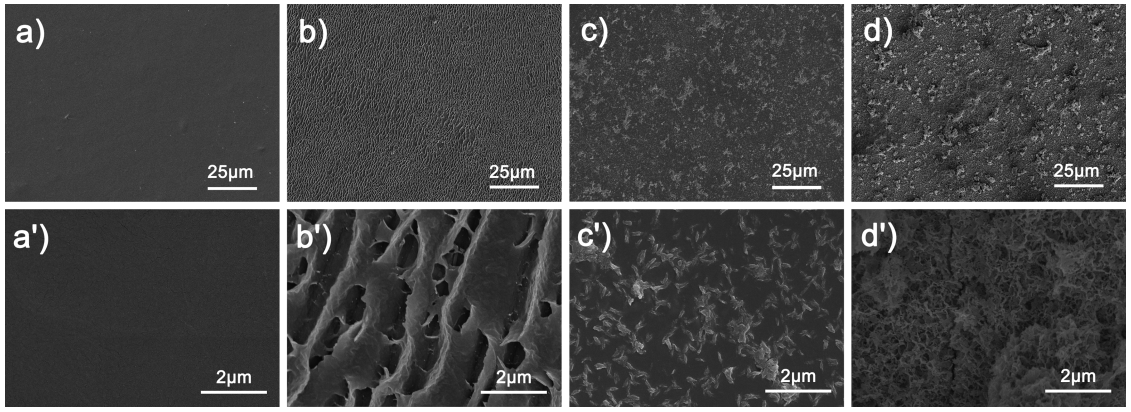

Figure 2. Surface morphology of (a, a′) PCLS, (b, b′) PCLT, (c, c′) PCLM, and (d, d′) PCLTM at various magnification indices.

exhibit bioinertness, with an absence of cell-anchorage, bioactive moiety, and hydrophilic groups.[18] Endowing these materials with bioactive properties remains challenging.[19,20] Constructing a biomimetic surface onto polyesters may be a feasible strategy for directing their biological functions.[20−22]

In natural bone tissues, the biological behavior of bone tissue cells is regulated by cell-ECM interactions.[23] A major part of the bone ECM comprises inorganic components (~65 wt %), mainly hydroxyapatite (HA). Accumulating evidence has demonstrated that HA-based biomaterials effectively promote the osteogenic differentiation and osteogenesis of MSCs.[24−26] Currently, three main approaches have been identified for surface mineralization: (i) incubation in simulated body fluid (SBF) to allow for calcium phosphate (CaP) deposition, (ii) chemical deposition by alternative exposure to Ca^{2+} and PO_4^{3-} solutions, and (iii) seeding osteogenic lineages onto the scaffold surface to secrete mineralized ECM followed by decellularization.[27] However, these biochemical modifications may not be suitable for aliphatic polyesters as the bioinert surface of aliphatic polyesters lacks a hydrophilic group, and excessive chemical modification may alter the original properties of aliphatic polyesters.

Generally, surface mineralization is initiated from apatite nuclei, which grow by consuming CaO and P_2O_5 from the surrounding fluid.[28] Thus, providing sufficient crystallization sites for apatite nuclei is necessary for surface biomineralization. In our previous study, we proposed the use of surface-directed epitaxial crystallization to construct a nano-topological structure on the PCL substrate.[29] Uniform edge-on lamellae developed from the substrate following the preferred crystallographic match. The thickness, periodic distance, and root-mean-square nano-roughness of the epitaxial lamellae were tunable by changing the crystallization parameters. We hypothesized that this specific nano-topological pattern with an increased surface area and roughness could provide more mineralized crystallization sites for mimicking the natural bone microenvironment. Thus, in this study, we explored the possibility of biomineralization on the PCL substrate with nano-topology (Figure 1). We first investigated the effects of the nano-topology structure on mineralization. Next, bone marrow MSCs (BMSCs) were used to evaluate the osteogenic properties of the topology-mineralization surface. Cell proliferation experiments, alkaline phosphatase, mineralization quantitation, and osteogenic mRNA detection were performed to investigate the biological effects of the biomineralized surface. This study provides a plausible method for efficiently biomineralizing the surface of aliphatic polyesters, addressing the problem of bioinertness of different aliphatic polyester scaffolds for use in clinical applications.

https://doi.org/10.1021/acsomega.1c03462
ACS Omega 2021, 6, 21792−21800

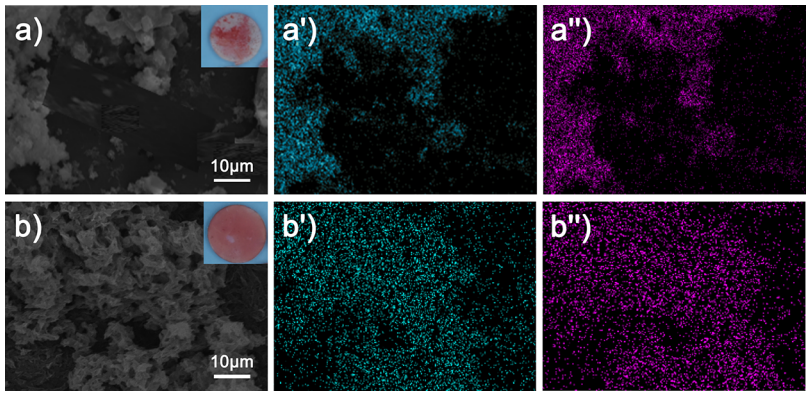

Figure 3. Scanning electron microscopy images (a, b) and X-ray energy-dispersive spectroscopy elemental mapping images of Ca and P of PCLM (a′, a″) and PCLTM (b′, b″). Insets represent digital photographs of the sample stained by alizarin red.

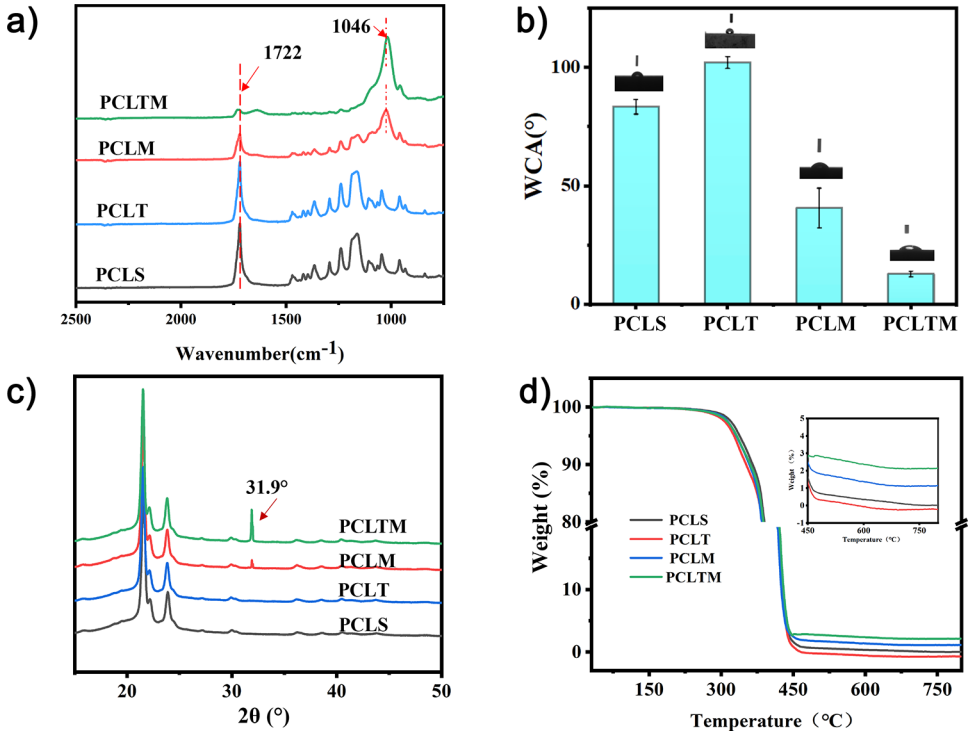

Figure 4. Surface properties of different groups: (a) Fourier transform infrared spectra, (b) water contact angles, (c) X-ray diffraction spectra, and (d) thermogravimetric analysis curves of PCLS, PCLT, PCLM, and PCLTM.

RESULTS AND DISCUSSION

Surface Morphology. The procedure of surface epitaxial nano-topography-facilitated biomineralization is illustrated in Figure 1. The surface of PCLS was smooth, as shown in Figure 2a,a′. Epitaxial formation of the uniform nano-topology was observed on the sample surface (Figure 2b). At higher magnification (Figure 2b′), the nanoridge was found to be composed of edge-on PCL lamellae and showed increased surface roughness. Because of the low surface energy, deposition of CaP on the smooth PCLS was difficult. Sparse precipitates were observed on the PCLM surface (Figure 2c) along with immature mineralization (Figure 2c′). In contrast, a large amount of mineralization precipitates was observed on PCLTM (Figure 2d). Upon immersion in the biomimetic solution with calcium and phosphate, the nano-topology provided nucleation sites for CaP crystal growth. The mineralized coating covered PCLTM homogeneously and showed a connected and compact petal-like morphology (Figure 2d′). As a result, biomimetic mineralization was considerably promoted by epitaxial crystallization.

Figure 3 shows the scanning electron microscopy images and EDS elemental mapping images of Ca and P for PCLM and PCLTM. The insets represent the digital photographs of the sample stained with alizarin red, which combines with calcium ions to produce strong chelates. Greater mineralization on PCLTM was observed with stronger dyeing. Additionally, EDS elemental mapping was performed to detect the distribution of Ca and P. Figure 3a′,a″ shows local agglomeration of Ca and P on PCLM, forming a coating on only a part of the surface, whereas they were uniformly distributed and covered the entire surface of PCLTM (Figure 3b′,b″). The nano-topography was conducive to hydroxyapatite (HA) deposition.

https://doi.org/10.1021/acsomega.1c03462
ACS Omega 2021, 6, 21792−21800

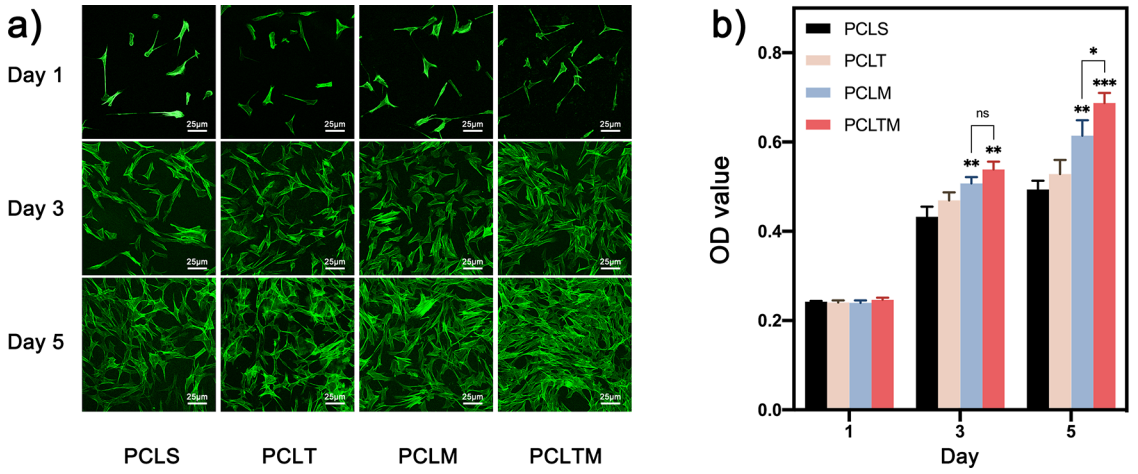

Figure 5. Adhesion and proliferation of BMSCs: (a) fluorescence staining showing the morphology and cell density of BMSCs under CLSM; (b) viability of BMSCs on different substrates after 1, 3, and 5 days of cultivation. Data represent the mean ± SD ($n = 3$), *$p < 0.05$, **$p < 0.01$, ***$p < 0.001$.

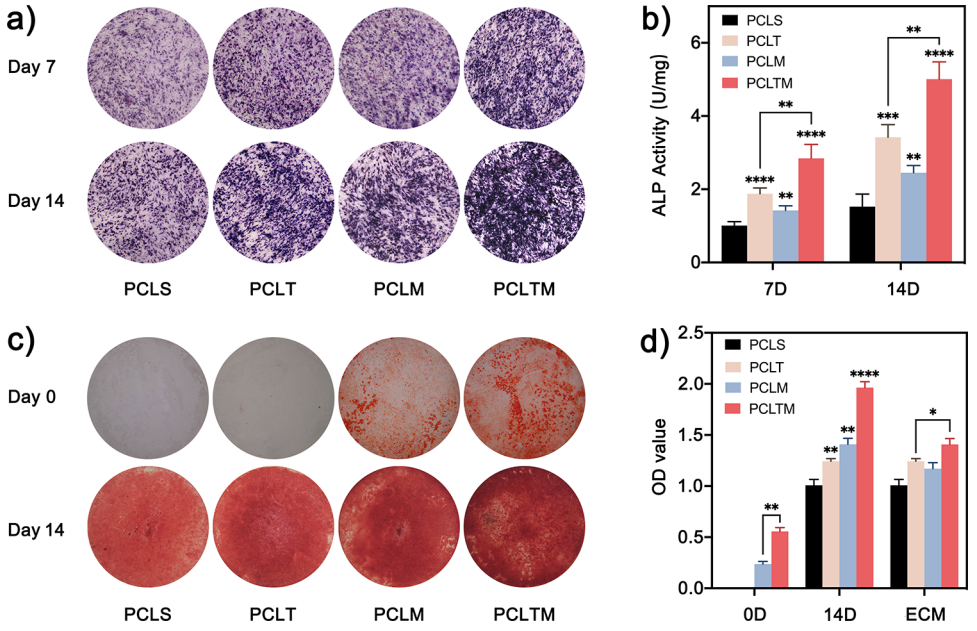

Figure 6. Osteogenic differentiation of BMSCs on substrate surfaces. (a) ALP product staining of BMSCs cultured for 7 and 14 days; (b) ALP activity quantitation of BMSCs cultured for 7 and 14 days; (c) mineralization staining of different substrate surfaces on days 0 and 14; (d) mineralization quantitation of different substrates: the 0D group reflects the initial surface biomineralization on different surfaces, and the 14D group reflects the total mineralization on different substrates on day 14. The ECM refers to the mineralization secreted by BMSCs obtained by subtracting the initial mineralization volume (0D) from the total mineralization volume (14D). Data represent the mean ± SD ($n = 4$), *$p < 0.05$, **$p < 0.01$, ***$p < 0.001$.

Figure 4a shows the Fourier transform infrared spectrum of the samples. PCLS showed a C═O peak of PCL at 1722 cm^{-1}. In addition, the same spectrum of PCLT indicated an unchanged chemical composition, verifying the occurrence of homogeneous epitaxial crystallization. After biomimetic mineralization, both PCLM and PCLTM showed the characteristic peak of HA at 1046 cm^{-1}, whereas the characteristic peaks of PCL were weakened. Particularly, the characteristic peaks of PCL were nearly absent from those of PCLTM, confirming the formation of a dense mineralized layer. Figure 4b shows the X-ray diffraction pattern of the decorated surface. Compared with PCLM, HA, with a characteristic peak of 31.9°, was more obvious on PCLTM, in accordance with the results shown in Figure 3a. The mineralized layer significantly reduced the water contact angle of the surface (Figure 4c), which decreased from 83 ± 1.8° for PCLS to 46.7 ± 5.6° for PCLM and from 102 ± 2.0° for PCLT to 21.1 ± 1.5° for PCLTM. The residual weight fraction observed in the thermogravimetric analysis curves reflects the HA mineralization level (Figure 4d). The residual amount of PCLTM (2.78%) was double that of PCLM (1.33%). This further demonstrates that the surface nano-topography promotes biomimetic mineralization.

Adhesion and Proliferation of BMSCs on the Biomineralized Surface. The morphology of BMSCs was marked using phalloidin, which can clearly display the cytoskeleton under confocal laser scanning microscopy (Figure 5a). After seeding, cells perceive the surface microenvironment

https://doi.org/10.1021/acsomega.1c03462
ACS Omega 2021, 6, 21792−21800

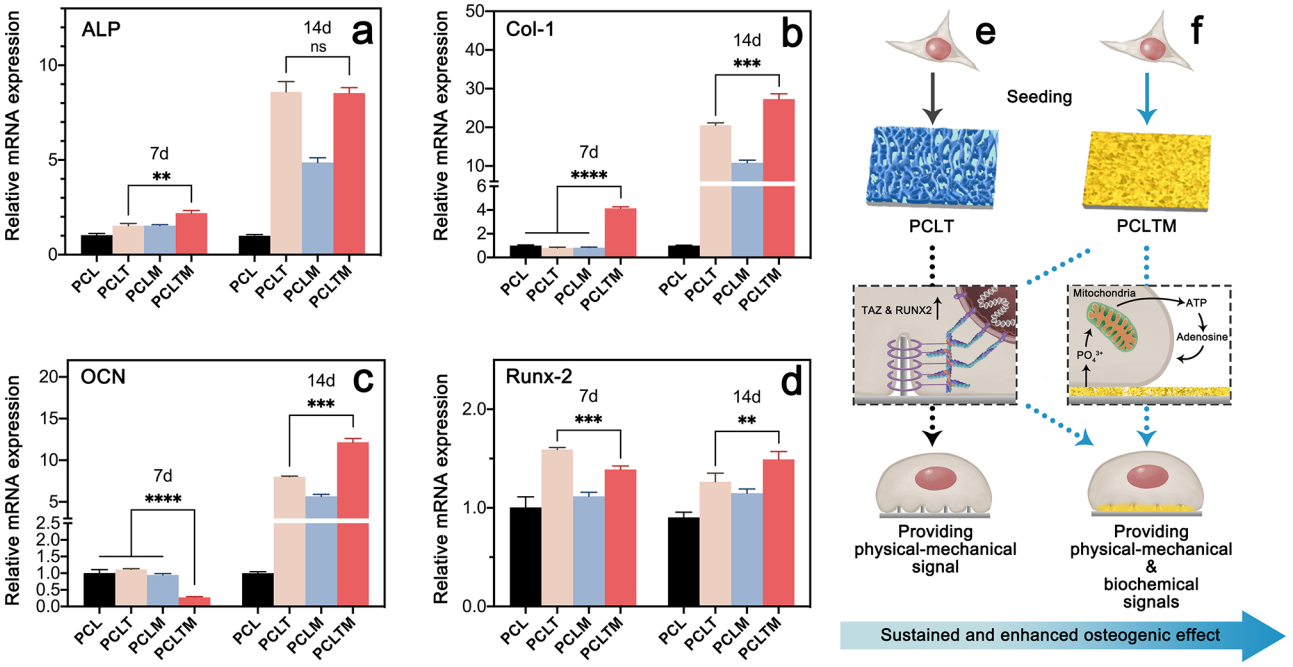

Figure 7. qRT-PCR results: expression of (a) ALP, (b) Col-I, (c) OCN, and (d) Runx-2 in BMSCs on different substrates after 7 and 14 days of cultivation; (e, f) underlying mechanism of the osteogenic effect of PCLT and PCLTM. Data represent the mean ± SD (n = 3), *p < 0.05, **p < 0.01, ***p < 0.001.

and transform their morphologies, greatly influencing their fate, particularly their differentiation.[30,31] After seeding for a day, the cells from all four groups were evenly dispersed without any apparent difference in density. After continuous cultivation for 3 days, cell proliferation was observed in the four groups. Cell densities in the mineralization groups (PCLM and PCLTM) exceeded those observed in PCLS and PCLT. On day 5, BMSCs in different groups proliferated, reaching higher cell densities. PCLTM showed the highest proliferation rate and near-saturated cell density. Because of direct contact with the topology structures, the cells on PCLT showed slight elongation, whereas the cells on the biomineralization surface showed greater dispersion. This is consistent with the surface hydrophilicity in the different groups. The excellent hydrophilicity of PCLTM provided a desirable surface for cell migration and proliferation. Furthermore, the adhesion and migration of cells associated with bone production on a biomaterial surface are mediated via integrins.[32] Protein−surface interactions not only depend on surface physicochemical properties (e.g., topology and roughness) but also are correlated with adsorbed proteins. CaP has a high adsorption capacity for serum proteins, providing more adhesive sites for seeding cells.[24,33]

The CCK-8 assay was performed to quantitatively investigate the viability and proliferation of BMSCs (Figure 5b). On the first day after seeding, there was no significant difference between the four groups as newly seeded cells had not entered the exponential growth period. However, there was also no extra cytotoxicity caused by the biomineralized surface. After cultivation for 3 days, cell viability in the PCLT, PCLM, and PCLTM groups exceeded that in the control group (PCLS), with significant results observed for PCLM and PCLTM. After cultivation for 5 days, a slight increase was observed among the four groups, indicating that the cell density was close to saturation and that cell proliferation had entered a plateau period. During this period, cell viability in PCLTM showed the greatest increase, exceeding that of PCLM (p < 0.05). This is because the mineralized layer on PCLTM renders the PCL surface hydrophilic and provides surface roughness for cell proliferation.

Osteogenic Differentiation of BMSCs on the Biomineralized Surface. Bone defect repair is a cellular cascade reaction involving various cells, and the bone-producing cell lines are mainly derived from BMSCs.[34] Directing osteogenic differentiation of BMSCs is critical for designing bone tissue engineering scaffolds. The osteogenic effect of PCLTM was evaluated by measuring ALP activity, which is an early osteogenic differentiation marker. Compared with PCLS, denser and deeper nodules were observed on the PCLT surface, and PCLTM exhibited the strongest ALP product staining (Figure 6a). Compared with the results observed after cultivation for 7 days, those at 14 days showed enhanced ALP activities that reflect further osteogenic differentiation of BMSCs. ALP activity showed the same trends (Figure 6b). Compared with that of PCLS, the ALP activities of PCLT, PCLM, and PCLTM were significantly enhanced. PCLT showed higher activity than PCLS and PCLM, which was ascribed to the nano-topology that provided physical cues for cell differentiation.[35] Notably, PCLTM showed higher activity than PCLT after cultivation for both 7 and 14 days. This result indicates that a single physical-mechanical entity has a limited ability to reflect the full biological scope of the natural bone ECM, whereas biomimetic modification is a good strategy for addressing this problem.[31] Through biomimetic mineralized modification, the PCLTM surface closely mimics the natural bone microenvironment, thereby exhibiting strong osteogenic effects.

Mineralization of BMSCs cultured on different substrate surfaces was measured by alizarin red staining. On day 0, no staining was observed on PCLS and PCLT. A small number of mineralized crystals were found on PCLM, and increased mineralized crystals were observed on PCLTM (Figure 6c).

https://doi.org/10.1021/acsomega.1c03462
ACS Omega 2021, 6, 21792−21800

After cultivation for 14 days, mineralization was observed in all four groups. The staining results showed that PCLM and PCLTM both exhibited mineralization, attributed to BMSCs, and initial biomineralization. To better quantify the osteogenesis effect of BMSCs, 10% cetylpyridinium chloride was used to dissolve the alizarin red stain followed by measurement of the optical density values. As shown in Figure 6d, the number of mineralized crystals formed on the PCLTM surface was approximately twice (2.34-fold) that on PCLM on day 0. After cultivation for 14 days, apparent mineralization increases were observed in the four groups, which is consistent with the staining results. The ECM group represented minerals secreted by BMSCs during differentiation, which was calculated by subtracting the initial mineralization on the substrate from the total mineralization observed in 14 days. PCLTM still showed the greatest increase in mineralization compared to the other groups. The results reveal that surface biomineralization promoted by nano-topography significantly enhanced osteogenesis.

The expression of osteogenesis-related genes (ALP, Col-1, Runx-2, and OCN) was analyzed via RT-PCR (Figure 7). On day 7, expression of the ALP gene presented a similar trend as the ALP activity expression shown above. This activity was upregulated by 2.2-fold (PCLTM) and 1.53-fold (PCLT) compared to that of PCLS. Additionally, the expression of Col-1 was upregulated in the PCLTM group (4.1-fold) compared to those in the other groups. The expression of Col-1 indirectly reflected the production of type I collagen, which constitutes the main component of the natural bone ECM. Furthermore, it demonstrated that BMSCs constantly differentiated into osteoblasts, which are the chief bone-making cells and main producers of type I collagen.[36] Thus, this result highlights the superior osteogenic effect of PCLTM. The expression levels of OCN for PCLTM were downregulated, possibly because OCN is a later-stage osteogenic marker of BMSCs.[34] Runx-2 is an osteogenic gene expressed in pre-osteoblasts, reflecting the preliminary osteogenic differentiation of BMSCs. This gene was upregulated by 1.6-fold (PCLT) and 1.39-fold (PCLTM) compared to that in the control group (PCLS). Compared to PCLTM, PCLT exhibits an early-stage osteogenic effect. In our previous study, we confirmed that this topology structure can provide physical signals upregulating TAZ and Runx-2 to promote osteogenic differentiation[29] (Figure 7e). However, such a physical-mechanical signal is short-lived in BTE application; the nano-topology on PCLT may be constantly decreased during the biodegradation process.[37] Thus, compared with PCLTM, PCLT mainly provides an immediate and early osteogenic effect, and further mineralized modification (PCLTM) may result in a long-term effect and better reliability in BTE applications.

As cultivation was extended to 14 days, the expression of osteogenesis-related genes showed a similar trend. Compared with the PCLS group, nano-topography modification (PCLT) resulted in significant upregulation of osteogenesis-related genes, which was also significantly higher than that observed in the biomineralization group (PCLM). Notably, the topology-mineralization group (PCLTM) showed the most significant upregulation of osteogenesis-related genes. Apart from ALP expression showing no significant difference compared to that observed with PCLT, the expression of other osteogenesis-related genes was significantly higher than in the other groups. This result indicates that PCLTM has desirable osteogenesis effects over the long term, highlighting the advantages of this modification method. Several studies have demonstrated the underlying osteogenic mechanism of biomineralization modification. Compared to the nano-topography in PCLT, which mainly provides cells with physical signals, the biomineralization layer can deliver both physical-mechanical and biochemical signals to the seeded cells. The application of SBF immersion can form a CaP nanostructure layer onto a biomaterial surface, which can significantly enhance surface roughness.[38] A rougher surface can affect cell adhesion, migration, and morphology, thereby regulating cytoskeletal tension. This tension can further activate the nuclear transcription factors YAP/TAZ via the cytoskeleton, which binds to the osteogenic transcriptional factor Runx-2, finally promoting osteogenic differentiation.[39] Additionally, biomineralization can provide biochemical signals by releasing Ca and P ions. Uptake of phosphate can promote the synthesis of ATP in mitochondria. The release and degradation of ATP can produce adenosine, which further activates adenosine receptors on the cell surface through the autocrine/paracrine pathway, thereby promoting cell osteogenic differentiation.[26] This biochemical signal results from the constant release of calcium phosphate ions, and its osteogenic effects may be sustainable (Figure 7f).

Our findings clearly demonstrate that constructing a biomimetic mineralized layer onto a nano-topology surface may be an efficient route for bioactivation of an inert polymer surface. Furthermore, it is of use to transfer 2D surface modification to 3D porous scaffolds, which are foundational for BTE applications. Most reported surface modification methods may be difficult to reproduce in 3D scaffolds, particularly those with complex structures. The immersion-evaporation modification method used in this study is theoretically not greatly affected by the scaffold structure. The nano-topography and CaP layer were mediated by the growth solution, which can readily infiltrate arbitrary pores and surfaces of the scaffolds. When applied to the 3D scaffold, similar modification results were observed as with a 2D substrate (Figure S2). This modification approach is applicable for decorating polymer BTE scaffolds with desirable morphological structures and mechanical properties while maintaining suitable biological properties. In the face of critical bone defects in clinical practice, researchers may use this approach to fabricate biomimetic scaffolds and implant them into the bone defect area to promote bone healing and new bone formation. At the same time, with the biodegradation of the internal polymer materials, the entire bone tissue engineering scaffold will be further replaced by natural bone tissues without leaving any synthetic materials or scars. Therefore, this simple surface biomimetic modification would bring a very effective bone repair effect.

CONCLUSIONS

In summary, the nano-topography epitaxial crystallization and SBF immersion-evaporation method successfully constructed a biomimetic mineralized layer onto a bioinert PCL substrate. An adequate and dense mineralized coating formed on the nano-topographical surface. Proliferation and osteogenic differentiation of BMSCs were significantly promoted by the mineralized surface. The biomimetic mineralized surface provided BMSCs with both physical-mechanical and biochemical osteogenic signals, resembling the natural bone microenvironment. Hence, this surface modification strategy may be useful for bioactivation of inert polymer surfaces,

https://doi.org/10.1021/acsomega.1c03462
ACS Omega 2021, 6, 21792−21800

demonstrating significant potential in bone tissue engineering and other related biomedical applications. It may be possible to combine this bioactive surface and biomimetic method with the bone structure biomimetic scaffold to provide a more suitable osteogenic environment for cells at the bone regeneration site.

EXPERIMENTAL SECTION

Materials. PCL (600C, M_η = 60,000 g/mol) was purchased from EASON Technology Co., Ltd. (Shenzhen, China). Tris-hydroxymethyl aminomethane (Tris), acetic acid (AcOH, AR-grade), and all other reagents were purchased from the Chengdu Kelong Chemical Reagent Factory (Chengdu, China).

Sample Preparation. *Topological Structure Construction.* PCL sheets were fabricated by compression molding at 100 °C and 10 MPa. The prepared sheets were annealed at 50 °C for 12 h. The nano-topography-based structure was obtained via epitaxial crystallization. Briefly, the annealed PCL sheets were immersed in prepared 0.5% w/v PCL solution (77/23 v/v acetic acid/water solution) for 10 min followed by evaporating the solvent naturally at room temperature. The detailed procedures were described in a previous study.[29] The topological sheet was used as the substrate for biomineralization.

Biomimetic Mineralization. Supersaturated 10× SBF was prepared as reported previously.[27] It consisted of 58.50 g of NaCl, 0.37 g of KCl, 3.68 g of $CaCl_2{\cdot}2H_2O$, 1.02 g of $MgCl_2$, and 1.2 g of NaH_2PO_4 to 1000 mL of deionized water. The topological sheets were soaked in 10× SBF solution, and 0.1 mM/L Tris-solution was added as a buffer to regulate the pH at 7.4. The mineralization process was performed for 10 h at 37 °C, and the supersaturated 10× SBF solution was replaced at 5 h. The samples were removed and rinsed with deionized water to remove minerals not bound to the substrates. For comparison, the same mineralization procedure was performed on the smooth PCL sheet. The smooth sheet, topological sheet, and structure obtained after mineralization on the smooth and topological surfaces are abbreviated as PCLS, PCLT, PCLM, and PCLTM, respectively.

Sample Characterization. The surface morphology of the sheets was observed by field-emission scanning electron microscopy (Nova Nano450, FEI, Hillsboro, OR, USA) at an acceleration voltage of 5 kV. X-ray energy-dispersive spectroscopy (EDS; Inca Energy 200, Oxford Instruments, Oxford, UK) was used to detect the distribution of Ca and P elements. Fourier transform infrared spectroscopy (Nicolet 6700, Thermo Fisher Scientific, Waltham, MA, USA) was performed in the range of 650−4000 cm^{-1} at a resolution of 2 cm^{-1}. The mineral phase on the substrates was evaluated by X-ray diffraction (Ultima IV, Rigaku, Tokyo, Japan) analysis. Hydrophilicity was measured using a contact angle goniometer (DA 30, Krüss, Hamburg, Germany), and the average value of five specimens per group was measured.

Cell Culture. BMSCs were extracted from 2 week old male Sprague−Dawley rats.[40] Briefly, the femur and tibia of euthanized rats were surgically removed, and the bone marrow cavity was washed with basic medium to obtain BMSCs. Flow cytometry was used to identify the cell type (Figure S1). An MEM-Alpha basic (Gibco, Grand Island, NY, USA) containing 10% fetal bovine serum (Gibco) and 1% antibiotic solution (penicillin and streptomycin) was used for culture. Cells obtained after passages 3−5 were used for subsequent experiments. Animal experiments were approved by the Sichuan Experimental Animal Management Committee (Sichuan, China).

Cell Morphology. The morphology of BMSCs was observed by fluorescence staining. BMSCs were cultured on the samples for 1, 3, and 5 days at a seeding density of 10,000 cells/cm^2, rinsed with phosphate-buffered saline (PBS), and fixed in 4% paraformaldehyde. The cells were then incubated with phalloidin and finally imaged by confocal laser scanning microscopy.

Cell Viability Assay. Cell viability was determined using cell counting kit-8 (CCK-8) after culturing the cells for 1, 3, and 5 days at an initial seeding density of 10,000 cells/cm^2. At the abovementioned time point, the culture medium was collected according to the manufacturer's instructions (CK04, Dojindo, Kumamoto, Japan) to determine relative intracellular lactate dehydrogenase concentrations. After washing with PBS, cells on the samples were incubated with 10% CCK-8 solution at 37 °C for 2 h and then the solution absorbance was read at 450 nm.

Alkaline Phosphatase (ALP) Activity. BMSCs (20,000 cells/cm^2) were seeded onto the sample surface. After the cell culture density reached ∼70%, an osteogenic induction medium was added for further cultivation. After incubation for another 7 or 14 days, the samples were washed and treated with cell lysis buffer (P0013J, Beyotime, Shanghai, China). ALP activity was evaluated by measuring the absorbance at 405 nm. The results were normalized to the total protein contents, which were tested by a bicinchoninic acid protein assay (P0321M, Beyotime, Shanghai, China). A 5-bromo-4-chloro-3-indolyl-phosphate/nitro blue tetrazolium ALP color development kit (C3206, Beyotime, Shanghai, China) was used to stain the ALP product of BMSCs.

Extracellular Matrix Mineralization. Mineral deposition was evaluated by alizarin red staining. The initial biomineralization volume was measured on the substrates. The osteogenesis effect was evaluated on day 14. Briefly, BMSCs were seeded onto the samples. After the cell culture density reached ∼70%, the medium was replaced with the osteogenic induction medium. On day 14, the samples were washed and fixed in 4% paraformaldehyde and then stained with 2% alizarin red. Next, staining was desorbed with 10% cetylpyridinium chloride and absorbance was measured at 560 nm.

Quantitative Real-Time (qRT) Polymerase Chain Reaction (PCR) Assay. The expression of osteogenesis-related genes was detected by the qRT-PCR assay. BMSCs (20,000 cells/cm^2) were cultured on the sample surface. When the cell culture density reached ∼70%, the culture medium was replaced with the osteogenic induction medium. On days 7 and 14, the cells were digested from the material surface with Trypsin−EDTA (1×, Phenol Red, Gibco), and total RNA was isolated using a total RNA extraction kit (RP1202, BioTeke, Beijing, China) and TB Green Premix Ex Taq II (RR082A, Takara, Shiga, Japan). qRT-PCR was performed with a QuantStudio 3 real-time PCR system (Thermo Fisher Scientific) using a PrimeScript RT reagent kit with a gDNA eraser (RR047A, Takara). The PCR thermal cycling parameters were as follows: 95 °C for 10 s followed by 40 cycles at 95 °C for 5 s, 60 °C for 15 s, and 72 °C for 30 s. Melting curve analysis of quantitative real-time PCR samples confirmed specific amplification. Gene expression was evaluated using the 2-ΔΔCt method. Glyceraldehyde-3-

https://doi.org/10.1021/acsomega.1c03462
ACS Omega 2021, 6, 21792−21800

phosphate dehydrogenase was used as a reference gene to standardize the expression levels of the target genes. The primer sequences are listed in Table S1.

Statistical Analysis. All measurements were performed in triplicate or quadruplicate, and the data are reported as mean ± standard deviation (SD). Statistical analysis was performed via *t* tests and one-way analysis of variance (ANOVA). A *p*-value < 0.05 was considered statistically significant.

■ ASSOCIATED CONTENT

Supporting Information

The Supporting Information is available free of charge at https://pubs.acs.org/doi/10.1021/acsomega.1c03462.

Identification of BMSCs by flow cytometry, surface modification in three-dimensional (3D) porous scaffolds, and primers used for qRT-PCR (PDF)

■ AUTHOR INFORMATION

Corresponding Authors

Jia-Zhuang Xu − *College of Polymer Science and Engineering and State Key Laboratory of Polymer Materials Engineering, Sichuan University, Chengdu 610065, China;* orcid.org/0000-0001-9888-7014; Email: jzxu@scu.edu.cn

Zhi-He Zhao − *State Key Laboratory of Oral Diseases, National Clinical Research Center for Oral Diseases, West China Hospital of Stomatology, Sichuan University, Chengdu 610041, China;* orcid.org/0000-0003-2955-1706; Email: zhzhao@scu.edu.cn

Authors

Guan-Yin Zhu − *State Key Laboratory of Oral Diseases, National Clinical Research Center for Oral Diseases, West China Hospital of Stomatology, Sichuan University, Chengdu 610041, China*

Ya-Hui Liu − *College of Polymer Science and Engineering and State Key Laboratory of Polymer Materials Engineering, Sichuan University, Chengdu 610065, China*

Wei Liu − *College of Polymer Science and Engineering and State Key Laboratory of Polymer Materials Engineering, Sichuan University, Chengdu 610065, China*

Xin-Qi Huang − *State Key Laboratory of Oral Diseases, National Clinical Research Center for Oral Diseases, West China Hospital of Stomatology, Sichuan University, Chengdu 610041, China*

Bo Zhang − *State Key Laboratory of Oral Diseases, National Clinical Research Center for Oral Diseases, West China Hospital of Stomatology, Sichuan University, Chengdu 610041, China*

Zi-Li Zheng − *College of Polymer Science and Engineering and State Key Laboratory of Polymer Materials Engineering, Sichuan University, Chengdu 610065, China*

Xin Wei − *College of Polymer Science and Engineering and State Key Laboratory of Polymer Materials Engineering, Sichuan University, Chengdu 610065, China*

Complete contact information is available at: https://pubs.acs.org/10.1021/acsomega.1c03462

Author Contributions

[§]G.-Y.Z. and Y.-H.L. contributed equally. The manuscript was written through contributions of all authors. All authors have given approval for the final version of the manuscript.

Notes

The authors declare no competing financial interest.

■ ACKNOWLEDGMENTS

This study was supported by the National Natural Science Foundation of China (81771048, 52022061, and 51773136), Research and Development Program, West China Hospital of Stomatology Sichuan University (RD-03-202012), and Sichuan Science and Technology Program (2020YFS0170).

■ ABBREVIATIONS

BMSCs, bone marrow mesenchymal stromal cells; BTE, bone tissue engineering; MSCs, mesenchymal stem cells; PCL, poly(ε-caprolactone); ECM, extracellular matrix; HA, hydroxyapatite; SBF, simulated body fluid; ALP, alkaline phosphatase; CCK-8, cell counting kit-8; qRT-PCR, quantitative real-time polymerase chain reaction

■ REFERENCES

(1) Dimitriou, R.; Jones, E.; McGonagle, D.; Giannoudis, P. V. Bone regeneration: current concepts and future directions. *BMC Med.* **2011**, *9*, 66.

(2) Younger, E. M.; Chapman, M. W. Morbidity at bone graft donor sites. *J Orthop Trauma* **1989**, *3*, 192−195.

(3) St John, T. A.; Vaccaro, A. R.; Sah, A. P.; Schaefer, M.; Berta, S. C.; Albert, T.; Hilibrand, A. Physical and monetary costs associated with autogenous bone graft harvesting. *Am J Orthop (Belle Mead NJ)* **2003**, *32*, 18−23.

(4) Finkemeier, C. G. Bone-grafting and bone-graft substitutes. *J Bone Joint Surg Am* **2002**, *84*, 454−464.

(5) Donati, D.; Di Bella, C.; Col angeli, M.; Bianchi, G.; Mercuri, M. The use of massive bone allografts in bone tumour surgery of the limb. *Current Orthopaedics* **2005**, *19*, 393−399.

(6) Henkel, J.; Woodruff, M. A.; Epari, D. R.; Steck, R.; Glatt, V.; Dickinson, I. C.; Choong, P. F. M.; Schuetz, M. A.; Hutmacher, D. W. Bone Regeneration Based on Tissue Engineering Conceptions - A 21st Century Perspective. *Bone Res* **2013**, *1*, 216−248.

(7) Sheehy, E. J.; Kelly, D. J.; O'Brien, F. J. Biomaterial-based endochondral bone regeneration: a shift from traditional tissue engineering paradigms to developmentally inspired strategies. *Mater Today Bio* **2019**, *3*, 100009.

(8) Zhu, T.; Cui, Y.; Zhang, M.; Zhao, D.; Liu, G.; Ding, J. Engineered three-dimensional scaffolds for enhanced bone regeneration in osteonecrosis. *Bioact Mater* **2020**, *5*, 584−601.

(9) Kirouac, D. C.; Zandstra, P. W. The systematic production of cells for cell therapies. *Cell Stem Cell* **2008**, *3*, 369−381.

(10) Rather, H. A.; Jhala, D.; Vasita, R. Dual functional approaches for osteogenesis coupled angiogenesis in bone tissue engineering. *Mater. Sci. Eng., C* **2019**, *103*, 109761.

(11) Zhu, G.; Zhang, T.; Chen, M.; Yao, K.; Huang, X.; Zhang, B.; Li, Y.; Liu, J.; Wang, Y.; Zhao, Z. Bone physiological microenvironment and healing mechanism: Basis for future bone-tissue engineering scaffolds. *Bioactive Materials* **2021**, *6*, 4110−4140.

(12) Koons, G. L.; Diba, M.; Mikos, A. G. Materials design for bone-tissue engineering. *Nat. Rev. Mater.* **2020**, *5*, 584−603.

(13) Takahashi, H.; Okano, T. Thermally-triggered fabrication of cell sheets for tissue engineering and regenerative medicine. *Adv. Drug Delivery Rev.* **2019**, *138*, 276−292.

(14) Dong, Y.; Liao, S.; Ngiam, M.; Chan, C. K.; Ramakrishna, S. Degradation behaviors of electrospun resorbable polyester nanofibers. *Tissue Eng Part B Rev* **2009**, *15*, 333−351.

(15) Zhao, D.; Zhu, T.; Li, J.; Cui, L.; Zhang, Z.; Zhuang, X.; Ding, J. Poly(lactic-co-glycolic acid)-based composite bone-substitute materials. *Bioact Mater* **2021**, *6*, 346−360.

(16) Zhao, X.; Han, Y.; Zhu, T.; Feng, N.; Sun, Y.; Song, Z.; Li, S.; Liu, J.; Ding, J. Electrospun Polylactide-Nano-HydroxyapatiteVanco-

mycin Composite Scaffolds for Advanced Osteomyelitis Therapy. *J. Biomed. Nanotechnol.* **2019**, *15*, 1213−1222.
(17) Cui, L.; Zhang, J.; Zou, J.; Yang, X.; Guo, H.; Tian, H.; Zhang, P.; Wang, Y.; Zhang, N.; Zhuang, X.; Li, Z.; Ding, J.; Chen, X. Electroactive composite scaffold with locally expressed osteoinductive factor for synergistic bone repair upon electrical stimulation. *Biomaterials* **2020**, *230*, 119617.
(18) Paragkumar, N. T.; Edith, D.; Six, J.-L. Surface characteristics of PLA and PLGA films. *Appl. Surf. Sci.* **2006**, *253*, 2758−2764.
(19) LeGeros, R. Z. Calcium phosphate-based osteoinductive materials. *Chem. Rev.* **2008**, *108*, 4742−4753.
(20) Richbourg, N. R.; Peppas, N. A.; Sikavitsas, V. I. Tuning the biomimetic behavior of scaffolds for regenerative medicine through surface modifications. *Journal of Tissue Engineering and Regenerative Medicine* **2019**, *13*, 1275−1293.
(21) Xiao, D.; Zhang, J.; Zhang, C.; Barbieri, D.; Yuan, H.; Moroni, L.; Feng, G. The role of calcium phosphate surface structure in osteogenesis and the mechanisms involved. *Acta Biomater.* **2020**, *106*, 22−33.
(22) Metwally, S.; Stachewicz, U. Surface potential and charges impact on cell responses on biomaterials interfaces for medical applications. *Mater Sci Eng C Mater Biol Appl* **2019**, *104*, 109883.
(23) Theocharis, A. D.; Skandalis, S. S.; Gialeli, C.; Karamanos, N. K. Extracellular matrix structure. *Adv. Drug Delivery Rev.* **2016**, *97*, 4−27.
(24) Ji, X.; Yuan, X.; Ma, L.; Bi, B.; Zhu, H.; Lei, Z.; Liu, W.; Pu, H.; Jiang, J.; Jiang, X.; Zhang, Y.; Xiao, J. Mesenchymal stem cell-loaded thermosensitive hydroxypropyl chitin hydrogel combined with a three-dimensional-printed poly(epsilon-caprolactone) /nano-hydroxyapatite scaffold to repair bone defects via osteogenesis, angiogenesis and immunomodulation. *Theranostics* **2020**, *10*, 725−740.
(25) Chai, Y. C.; Carlier, A.; Bolander, J.; Roberts, S. J.; Geris, L.; Schrooten, J.; Van Oosterwyck, H.; Luyten, F. P. Current views on calcium phosphate osteogenicity and the translation into effective bone regeneration strategies. *Acta Biomater.* **2012**, *8*, 3876−3887.
(26) Shih, Y.-R. V.; Hwang, Y.; Phadke, A.; Kang, H.; Hwang, N. S.; Caro, E. J.; Nguyen, S.; Siu, M.; Theodorakis, E. A.; Gianneschi, N. C.; Vecchio, K. S.; Chien, S.; Lee, O. K.; Varghese, S. Calcium phosphate-bearing matrices induce osteogenic differentiation of stem cells through adenosine signaling. *Proc. Natl. Acad. Sci. U. S. A.* **2014**, *111*, 990−995.
(27) Liu, W.; Lipner, J.; Xie, J.; Manning, C. N.; Thomopoulos, S.; Xia, Y. Nanofiber scaffolds with gradients in mineral content for spatial control of osteogenesis. *ACS Appl. Mater. Interfaces* **2014**, *6*, 2842−2849.
(28) Kokubo, T.; Yamaguchi, S. Simulated body fluid and the novel bioactive materials derived from it. *J Biomed Mater Res A* **2019**, *107*, 968−977.
(29) Yin, H. M.; Liu, W.; Huang, Y. F.; Ren, Y.; Xu, L.; Xu, J. Z.; Zhao, B.; Li, Z. M. Surface Epitaxial Crystallization-Directed Nanotopography for Accelerating Preosteoblast Proliferation and Osteogenic Differentiation. *ACS Appl. Mater. Interfaces* **2019**, *11*, 42956−42963.
(30) Kelly, D. J.; Jacobs, C. R. The role of mechanical signals in regulating chondrogenesis and osteogenesis of mesenchymal stem cells. *Birth Defects Res C Embryo Today* **2010**, *90*, 75−85.
(31) Hwang, M. P.; Subbiah, R.; Kim, I. G.; Lee, K. E.; Park, J.; Kim, S. H.; Park, K. Approximating bone ECM: Crosslinking directs individual and coupled osteoblast/osteoclast behavior. *Biomaterials* **2016**, *103*, 22−32.
(32) Anselme, K. Osteoblast adhesion on biomaterials. *Biomaterials* **2000**, *21*, 667−681.
(33) Zeng, H.; Chittur, K. K.; Lacefield, W. R. Analysis of bovine serum albumin adsorption on calcium phosphate and titanium surfaces. *Biomaterials* **1999**, *20*, 377−384.
(34) Lopes, D.; Martins-Cruz, C.; Oliveira, M. B.; Mano, J. F. Bone physiology as inspiration for tissue regenerative therapies. *Biomaterials* **2018**, *185*, 240−275.
(35) Dupont, S.; Morsut, L.; Aragona, M.; Enzo, E.; Giulitti, S.; Cordenonsi, M.; Zanconato, F.; Le Digabel, J.; Forcato, M.; Bicciato, S.; Elvassore, N.; Piccolo, S. Role of YAP/TAZ in mechanotransduction. *Nature* **2011**, *474*, 179−183.
(36) Long, F. Building strong bones: molecular regulation of the osteoblast lineage. *Nat Rev Mol Cell Biol* **2011**, *13*, 27−38.
(37) Raghunath, J.; Georgiou, G.; Armitage, D.; Nazhat, S. N.; Sales, K. M.; Butler, P. E.; Seifalian, A. M. Degradation studies on biodegradable nanocomposite based on polycaprolactone/polycarbonate (80:20%) polyhedral oligomeric silsesquioxane. *J Biomed Mater Res A* **2009**, *91*, 834−844.
(38) Costa, D. O.; Prowse, P. D. H.; Chrones, T.; Sims, S. M.; Hamilton, D. W.; Rizkalla, A. S.; Dixon, S. J. The differential regulation of osteoblast and osteoclast activity by surface topography of hydroxyapatite coatings. *Biomaterials* **2013**, *34*, 7215−7226.
(39) Yang, W.; Han, W.; He, W.; Li, J.; Wang, J.; Feng, H.; Qian, Y. Surface topography of hydroxyapatite promotes osteogenic differentiation of human bone marrow mesenchymal stem cells. *Mater. Sci. Eng., C* **2016**, *60*, 45−53.
(40) Lennon, D. P.; Caplan, A. I. Isolation of rat marrow-derived mesenchymal stem cells. *Exp Hematol* **2006**, *34*, 1606−1607.

https://doi.org/10.1021/acsomega.1c03462
ACS Omega 2021, 6, 21792−21800